Multifunctional pressure/temperature/bending sensor made of carbon fibre-multiwall carbon nanotubes for artificial electronic application

Wang, Hao; Tao, Jie; Jin, Kai; Wang, Xiaoyue; Dong, Ying

DOI
10.1016/j.compositesa.2021.106796

Publication date
2022

Document Version
Final published version

Published in
Composites Part A: Applied Science and Manufacturing

Composites: Part A 154 (2022) 106796

Contents lists available at ScienceDirect

Composites Part A

journal homepage: www.elsevier.com/locate/compositesa

Multifunctional pressure/temperature/bending sensor made of carbon fibre-multiwall carbon nanotubes for artificial electronic application

Hao Wang [a,b], Jie Tao [a,*], Kai Jin [c], Xiaoyue Wang [a], Ying Dong [a]

[a] College of Material Science and Technology, Nanjing University of Aeronautics and Astronautics, Nanjing 211106, China
[b] Faculty of Aerospace Engineering, Delft University of Technology, 2629 HS, Delft, Netherlands
[c] School of Materials Science and Engineering, Ocean University of China, Qingdao 266100, China

ARTICLE INFO

Keywords:
Carbon fibres
Carbon nanotube
Freeze casting
Hierarchical porous structure
Multifunctional composites

ABSTRACT

A flexible sensor with excellent pressure, temperature, and bending sensitivity is fabricated based on the conductive skeleton material with hierarchical porous structure. The conductive skeleton material is composed of carbon fibres (CFs) and multiwalled carbon nanotubes (MWCNTs), in which lay perpendicular to each other CFs are used as conductive frames, while MWCNTs are served as bridges to connect the CFs and increase the conductive network formation. Owing to the unique structure and the conductive materials, the as-prepared sensor exhibits a high-pressure sensing performance of 42.7 kPa (0–1 kPa), fast response, relaxation times of<100 ms, wide working range of 0–60 kPa, and high stability over more than 6000 cycles. Furthermore, the fabricated sensor presents a high thermal sensitivity of 2.46 °C^{-1} between 30 and 40 °C, excellent bending sensitivity of 95.5 % rad^{-1} in the working range of 0–180°, and great flexibility (over 1000 cycles), demonstrating its potential applications in multifunctional wearable electronics.

1. Introduction

Traditional electronic devices are usually composed of hard materials with poor flexibility and deformability, which limit their further application in deformable environments [1–2]. These drawbacks can be overcome by flexible, soft, and deformable electronic devices, which have attracted great interest with their potential applications in emerging fields such as wearable health devices [3], soft robots [4], and artificial intelligence [5–7]. Particularly the branch of flexible electronics dealing with electronic skins [7], flexible sensors [8], and human motion detection devices [9–11] is an attractive research area. Diverse flexible sensors have been developed to detect human motions, including heart or pulse beating [12–13], smiling [14], limb bending [15], etc., and play an important role in identifying substances in the environment and expanding human sensing behaviour. These sensors detect a specific physical change and collect signals to further help people control the physical changes in turn, thereby realizing human–machine interactions.

Many types of flexible sensors are derived from conductive materials, such as metal nanowires [16], carbon nanotubes (CNTs) [17], graphene [18–20], MXene [21,22], and porous foams [23]. The working mechanisms of wearable functional electronics are mainly based on changes in the resistance [24], piezoelectric properties [25], and capacitance [26]. In particular, due to their high aspect ratio, excellent conductivity, and high strength, carbon nanotubes (CNTs) can easily form a sensing conductive network with low weight ratio, which has attracted widespread attention [27]. Furthermore, CNTs have been commercialized and are relatively cheap compared to other conductive nanomaterials like metal nanowires, graphene and MXene [18–22]. For example, Jian et al. [28] developed a high-stability pressure sensor with superior sensing performance based on an aligned CNT/graphene mixed layer film and micro-structured polydimethylsiloxane (PDMS). Liu et al. [29] coated single CNTs onto braided cotton fabric by a dip-coating process to fabricate a pressure sensor with superior sensing performance and a wide working range. However, the above sensors usually work as a single mechanism. Hence, their detection range and sensitivity do not well meet the requirements of future multifunctional temperature, pressure and deformation sensing applications.

In this study, CFs and MWCNTs were selected as conductive materials due to their prices are lower than those of conductive materials such as commercial graphene-based nanocomposites and silver nanomaterials. The CFs-MWCNTs hierarchical porous network were constructed by the freezing casting method, and then encapsulated with the flexible matrix PDMS to prepare the multifunctional flexible sensor. The

* Corresponding author.
E-mail address: taojie@nuaa.edu.cn (J. Tao).

https://doi.org/10.1016/j.compositesa.2021.106796
Received 30 August 2021; Received in revised form 13 December 2021; Accepted 22 December 2021
Available online 28 December 2021

prepared sensor can independently recognize pressure, temperature, and bending physical changes. Also successfully detected human movements, including hand gestures, elbow bending, wrist bending, knee bending and heel pressure. Moreover, the 4 × 5 CFs-MWCNT flexible sensor array exhibits excellent pressure and temperature sensing capabilities. We believe that the proposed sensor can potentially be used in multifunctional integrated wearable electronic devices.

2. Experimental section

2.1. Materials

The carbon fibre (CF) tow was purchased from Weihai Guangwei Composite Material Co., Ltd., China (TZ700S-12 K, Unsized). Multi-walled carbon nanotubes (MWCNTs) were received from Nanjing XFNANO Materials Tech (Nanjing, China). Chitosan (C804726, Shanghai Macklin Biochemical Company) was selected as the solvent. Polydimethylsiloxane (PDMS) was used as the elastic substrate polymer matrix and was provided by Dow Chemical Shanghai Co., Ltd.

2.2. Preparation of hierarchical porous structure CFs-MWCNT conductive skeleton

First, chitosan (CS) solutions of multiwalled carbon nanotubes (MWCNTs) were prepared with different mass fractions. Therefore, 1 g of CS powder was dissolved in 50 mL of 2% (v/v) acetic acid aqueous solution to prepare a 2 wt% CS solution. Then, MWCNTs of different mass ratios were added, followed by ultrasonic stirring for two hours until a uniform dispersion without agglomeration was formed. Finally, MWCNT solutions with different mass fractions (2.5, 5, 7.5, 10, and 12 wt%) were obtained. Second, CF tows (12 K) were uniformly dispersed and thinned via tow-spreading technology [30], and then two CF layers were laid alternately and perpendicular to each other to form a CF network with a thickness of no more than 40 um. Then, the MWCNTs solution was uniformly sprayed onto the CF network via a spray process (**Figure S1**; nozzle diameter: 0.5 mm; spray air pressure: 4 bar), followed by freeze-drying (**Figure S2**). Finally, the samples were annealed to obtain porous CFs-MWCNTs conductive skeletons with different thicknesses (0.02–0.1 mm; interval: 0.02 mm). Conductive copper tape was pasted and fixed to the conductive skeleton to ensure a good electrical connection between the electrode and the sensing layer.

2.3. Fabrication of hierarchical porous structure CFs-MWCNT multifunctional sensor

The composite sensor was prepared by mixing the silicone elastomer PDMS (part A) and the crosslinking agent (part B) in a weight ratio of 10:1. Then, the CFs-MWCNT skeleton was soaked in the mixture while degassing in a vacuum oven for 20 min to remove bubbles. The PDMS-impregnated sample was placed in an aluminum mold with the dimensions of 30 × 30 × 1.5 mm (length × width × depth), and silicone elastomer was added to the mold. Then, the aluminum sheet was covered, and excess PDMS was pressed and extruded to ensure an equal senor thickness of 1.5 mm for all sensors. The obtained samples were cured at room temperature for 12 h and placed in a vacuum oven at 80 °C for 2 h. Based on the calculated weight difference before and after fabrication, the CF volume content of the sensor was approximately 2.7 vol%.

2.4. Fabrication of the multifunctional sensing array

Soft and transparent polyethylene terephthalate (PET) was used as the substrate, and the copper circuit was evaporated onto this substrate to form a 4 × 5 sensor pixel array. Then, 20 rectangular parallelepiped samples of the porous CFs-MWCNT skeleton were pasted on the circuit board using conductive tape, encapsulated in the flexible resin PDMS, and cured at room temperature for 72 h.

2.5. Characterization of the architecture

Sample morphologies were characterized by using a field emission scanning electron micro analyzer (TESCAN LYRA3, Bruker Nano, Berlin, Germany).

2.6. Performance test of sensor devices

The sensor was installed on a general material testing machine, which was connected to a digital multimeter (VC8246B, Voctor) for real-time monitoring of electrical changes for the pressure and bending test. A semiconductor heating device was used to apply different temperatures, and the electrical response of the sensor was detected by a digital multimeter (VC8246B, Voctor). To monitor human activity, sensor and tape were combined and installed on the active part of the human body, and changes in the electrical signal were recorded by the digital multimeter. The signal output of the flexible sensor array generated by different temperatures and loads was measured by the digital multimeter.

3. Results and discussion

3.1. Fabrication of the CFs-MWCNT composite sensor

The overall schematic illustration of the multifunctional carbon fibre (CF) sensor is presented in Fig. 1. The manufacturing process of the CF sensor (3 × 3 cm) can be divided into three parts (Fig. 1**a**). The detailed fabrication process is described in the experimental section. The two optical images shown in (Fig. 1**c, d**) exhibit the bending and twisting flexibility of the sensor. Cross-sectional scanning electron microscopy (SEM) images of the CFs-MWCNT scaffold (Fig. 1**e, f**) reveal that the MWCNTs acts as a bridge to connect neighboring CFs and form a porous network (**Figure S3 and Figure S4**). (Fig. 1**g**) shows the cross-sectional SEM images of the composite sensor, indicating that the thickness of the active sensing layer is about 40 μm. Furthermore, these images show that the elastic resin PDMS completely enveloped and filled the CFs-MWCNT scaffold, constituting a protective barrier to prevent external damage. Therefore, the CFs-MWCNT scaffold can serve as an effective insulation and safe substrate for skin contact applications.

3.2. Pressure sensing performance of the CFs-MWCNT composite sensor

To analyze the pressure response of the sensor, current measurements are performed at various pressure levels (Fig. 2**a**). As the pressure increased, the deformation of the entire conductive structure and the change of the contact area between CFs and MWCNTs produced more conductive paths. More specifically, when the pressure sensor is subjected to high pressure, the bulk resistance played a major role in the total resistance change. After unloading of the sensor, the conductive path length decreased, as the sensing layer recovered its original shape. Fig. 2**b** shows the current–voltage (IV) curves of the sensor under different pressures. From 0 to 50 kPa, the slope of the IV curve increases significantly with increasing pressure, which indicates that the sensor formed a favorable current response. The pressure sensitivity of the as-prepared sensor can be expressed by the following equation:

$$S_p = (\Delta I / I_O)/\Delta P \quad (1)$$

where ΔI is the corresponding current change, I_O is the initial current without pressure loading, and ΔP is the pressure change.

Figure S5a and S5b shows a comparison of the output voltage signals of sensors prepared with different amounts of MWCNTs. It can be found that when the mass fraction of MWCNTs is 7.5 wt%, not only the output voltage signal is stable but also the pressure sensitivity is higher

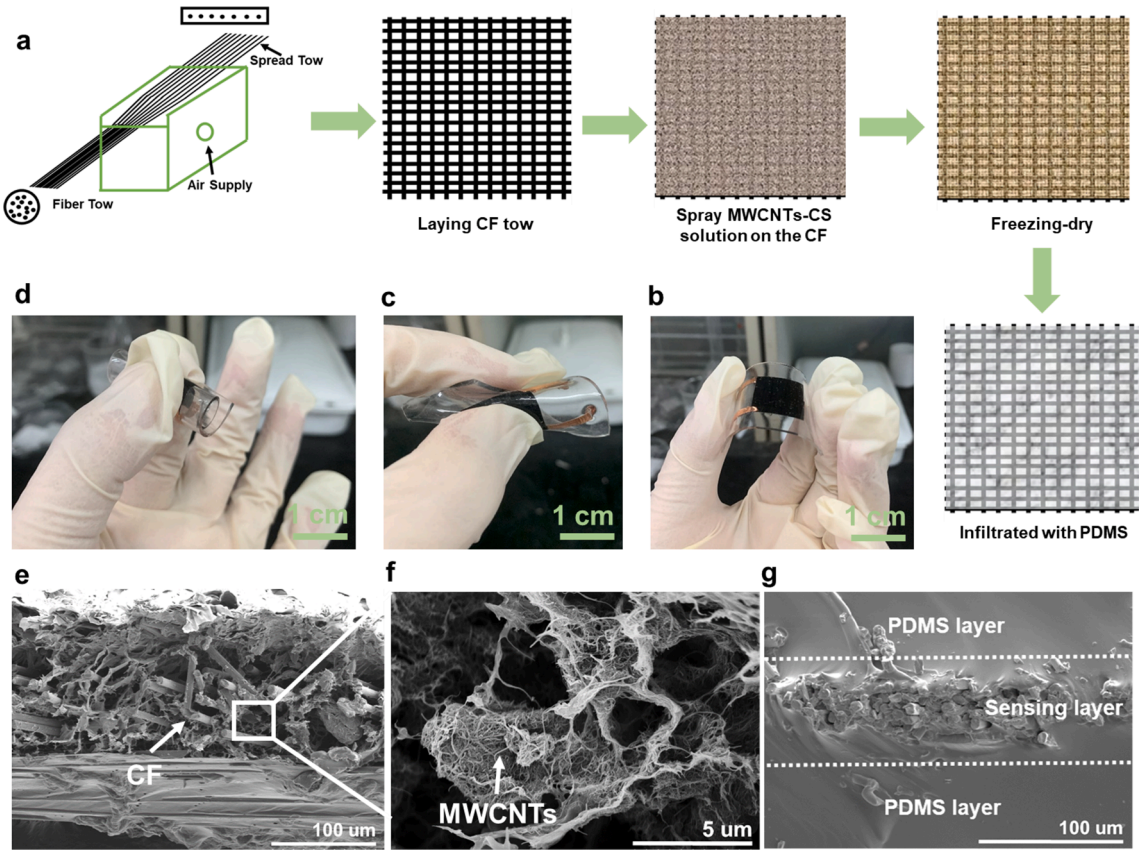

Fig. 1. Overall schematic illustration of the sensor. **a** Fabrication process of the CFs-MWCNT composite sensor; **b** Optical photograph of the CFs-MWCNT composite sensor; **c–d** Photograph of the CFs-MWCNT composite showing the bending and twisting flexibility; **e–f** Cross-section SEM images of the CFs-MWCNT scaffold; **g** Cross-sectional SEM images of the CFs-MWCNT composite sensor.

than that of other mass fraction sensors under the loading pressure of 5 kPa. In addition, a comparison of the output voltage signals of sensors with different sensing layer thicknesses but under the same pressure is shown in **Figure S5c, d**, demostrating that the pressure sensitivity increased relatively, as the thickness of the sensing layer increased from 0.02 to 0.08 mm. However, from the perspective of practical applications (e.g., electronic skin), a thinner thickness results in a higher flexibility in the sensor's application. However, the sensitivity of the sensing layer with a thickness of 0.02 mm is slightly lower than that with a thickness of 0.04 mm. Therefore, the mass fraction of MWCNTs is adjusted to 7.5 wt% to prepare the CFs-MWCNT composite sensor with a sensing layer thickness of 0.04 mm.

When pressure is applied to the sensor, the hierarchical porous structure of the sensing layer deformed, resulting in an increase of the contact interface and formation of more conductive paths. Furthermore, the contact area between the carbon fibers also changes with the pressure. The relative variation of the current ($\Delta I/I_O$) with changing pressure load is shown in (Fig. 2**c**). A higher sensitivity of 42.5 kPa^{-1} was measured when the pressure was below 10 kPa, which is obviously better than most reported sensor sensitivities (Fig. 2**h**) [31–38]. When the applied pressure is increased, the resistance decreased, and the results for the sensitivity range of 10–20 kPa are shown in (Fig. 2**c**). A slight change in the bulk resistance is observed due to the deformation of the bulk matrix under high pressure. The sensitivity dropped to 0.91 kPa^{-1} in the high-pressure range (20–60 kPa). The sensor has a continuous response, the electrical output signal is stable under the external load (i.e., pressure of 8 kPa), and it also has a fast response time and recovery time (<100 ms), as shown in (Fig. 2**d, e**). Dynamic pressures with different values are applied to the sensor to further verify the reliability of the pressure sensor and its wide detection range. The results are shown in (Fig. 2**f**). By increasing the pressure, the current gradually increasing and shows a stable and continuous wave, which indicates that the sensor can operate stably in a wide pressure range. Subsequent research further supported the sensor's long service life and high stability. As shown in (Fig. 2**g**), the sensor exhibites a highly stable electrical response under a pressure of about 12 kPa during 6000 loading and unloading tests with negligible changes, indicating excellent repeatability and durability. The sensor performance of the as-prepared sensor and those of other recently reported high-performance pressure sensors are compared in (Fig. 2**h**) and **Table S1** [31–38]. Most pressure sensors do not achieve high sensitivity and a wide linear range simultaneously through material selection and structural design. However, the as-prepared sensor shows a high sensitivity (42.5 kPa^{-1}) in a relatively low pressure region (<10 kPa), as well as a relatively high sensitivity (0.7 kPa^{-1}) in a relatively high pressure region (20–60 kPa). It also has good mechanical properties, with a tensile strength of approximately 45 MPa (**Figure S6**). Pressing and releasing the sensor by hand was tested, and the measured changes in the electrical response are shown in Video S1. This test prove that the as-prepared sensor has a fast and stable response under loading. The pressure sensing mechanisms of the sensor are illustrated in **Figure S7**. When the pressure increases, the hierarchical porous conductive network structure will undergo relatively large deformation. It will increase the contact area between the internal channels of the MWCNTs network from nanometer scale. From microscale, it will increase the contact area not only between the MWCNTs and the CF, but also between the CF and the CF. As a result, more conductive paths are formed in the network. Thus the sensor has a relative high pressure sensitivity of 42.5 kPa^{-1} when the pressure is below 10 kPa. Under continuous relatively heavy pressure (10–60 kPa), the hierarchical porous conductive network structure is slightly

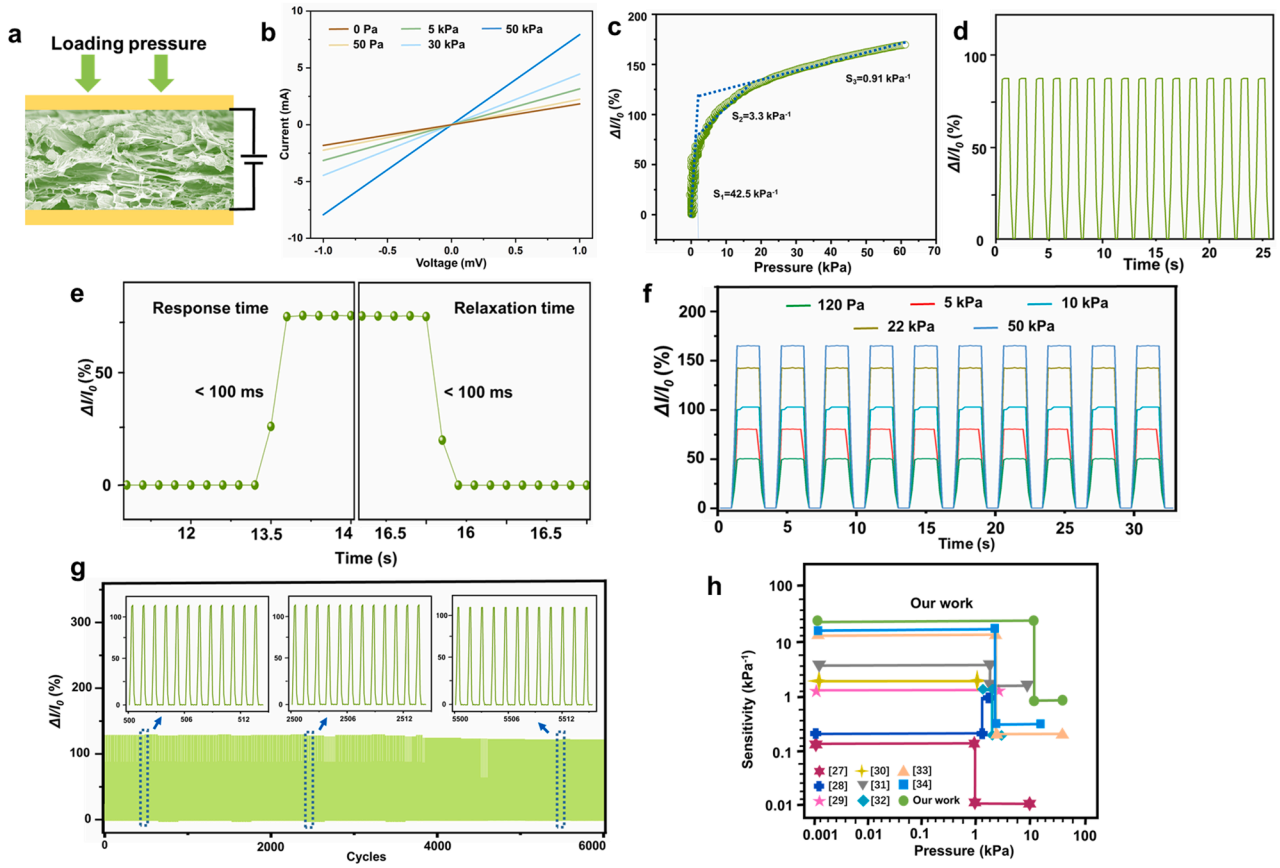

Fig. 2. Electrical characterization of the sensor's response to pressure. **a** Schematic illustration of the sensor under the loading pressure; **b** I-V curves of the sensor under different applied pressures; **c** current response ($\Delta I/I_0$) curves under the applied pressure; **d** current response over 15 cycles with a repeated loading pressure of 8 kPa; **e** dynamic response and recovery time; **f** cyclic current responses to various applied pressures; **g** durability test of the sensor over 6000 cycles under a repeated loading pressure of 12 kPa; the insets show the partial current response for the initial 10 cycles (left), middle 10 cycles, and final 20 cycles (right) of the stability test; **h** comparative study of recently reported pressure sensors.

deformed and the deformation becomes stable, which increases the contact area not only between MWCNTs and CFs, but also between CFs and CFs, resulting in an increase in the conductive paths. Therefore, the sensor has a relatively low pressure sensitivity.

3.3. Temperature and bending sensing performance of the CFs-MWCNT composite sensor

The responses of the as-prepared sensor to temperature and bending are characterized, as shown in Fig. 3. Here, we characterize the temperature change based on the voltage signal variation, as the detected current signal response is disturbed by the applied temperature [39]. The schematic of the sensor upon application of the temperature gradient is presented in (Fig. 3**a**). The thickness of the PDMS substrate affected the reaction time of the sensor, but it could not affect the sensitivity of the sensor to temperature. When the PDMS substrate is as thin as possible, the reaction time is predicted to be the fastest. The sensitivity of the temperature response is defined as follows:

$$S_T = (\Delta U/U_O)/\Delta T \quad (2)$$

where ΔU is the corresponding change in voltage, U_O is the initial voltage at room temperature, and ΔT is the temperature change.

Fig. 3**b** shows that the voltage changes continuously with increasing temperature, and the as-prepared sensor exhibits an instant voltage response. It is observed that the change in sensor resistance decreases with increasing temperature (Fig. 3**b**), indicating a negative temperature coefficient. The effect mechanism for the temperature on the sensor sensitivity can be explained by the following factors. In the initial temperature state, the MWCNTs are highly coiled and randomly distributed in the matrix. As the temperature rises, most of the highly distorted MWCNTs are completely stretched into wires, increasing the contact area between the MWCNTs and the CFs, benefiting from the thermodynamic expansion of PDMS, resulting in an increase in conductive paths and a decrease in resistance. Secondly, as temperature rises, the resistance will be affected by the thermal coefficients of each component of the sensing material [40]. When the temperature rises, due to the tunneling effect, delocalized electrons will be conducted in MWCNTs and CFs [41]. These electrons will jump between adjacent MWCNTs and CFs. The increase in electron jumps will increase the conductivity. The relative voltage change with the temperature is plotted in (Fig. 3**c**), showing that the voltage increases almost linearly with the temperature, and the corresponding sensitivity is 2.46% $℃^{-1}$ in the heating temperature range of 30–40 ℃. When the heating temperature exceeded 40 ℃, the linear voltage changes start to decelerate, and the corresponding sensitivity is 1.49% $℃^{-1}$. The sensitivity is higher than those of recently reported flexible sensors based on carbon nanotubes (CNTs) [42,43]. The temperature changed cyclically between room temperature (30.3 ℃) and 50 ℃, and the corresponding voltage response is shown in (Fig. 3**d**), revealing that the voltage response changed steadily with the temperature changes. These results show that the sensor can sensitively detect temperature changes based on a stable electrical signal response.

The bending response of the sensor is also examined, and the sche-

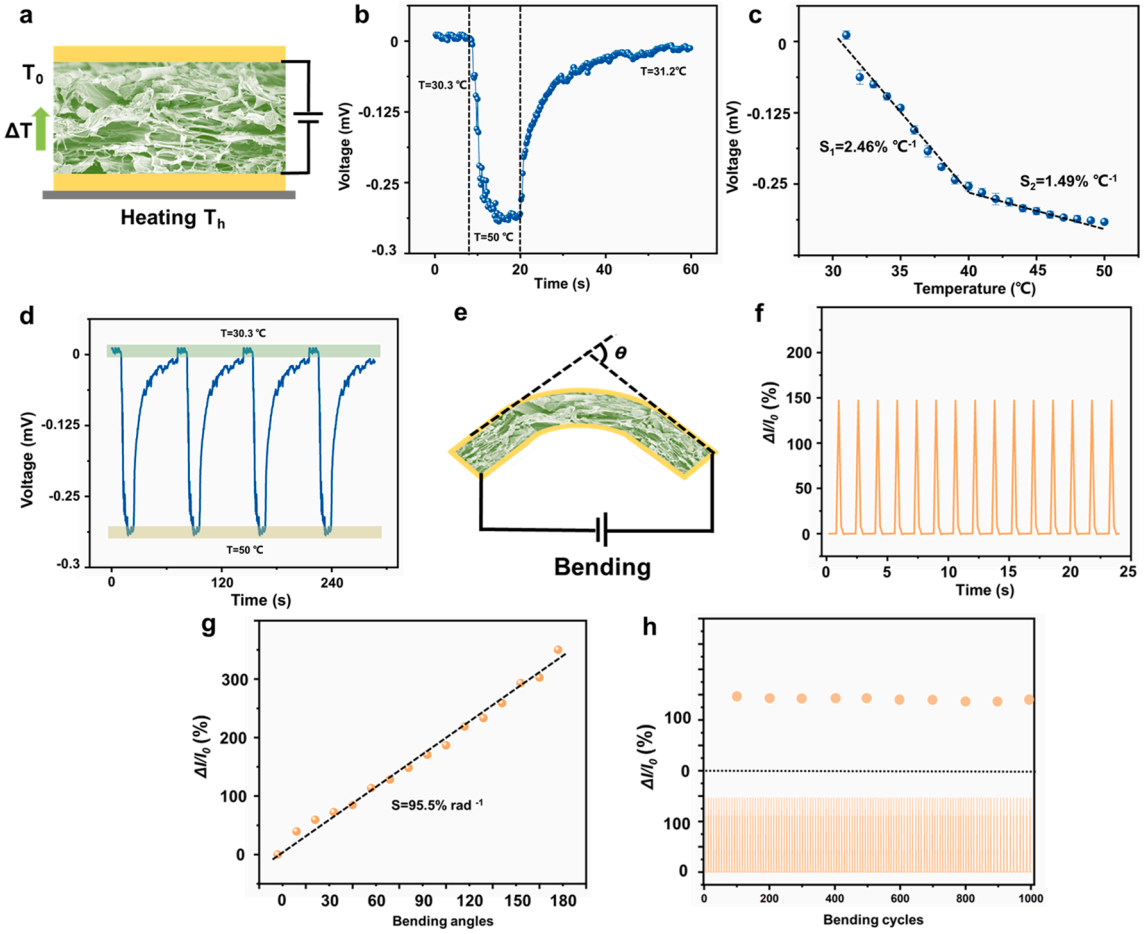

Fig. 3. Electrical characterization of the sensor in response to temperature and bending. **a** Schematic illustration of the sensor under application of the temperature gradient; **b** relative voltage changes in response to changes in the sensor temperature; **c** voltage response curves in the temperature range of 30.3 to 50 °C; **d** voltage response of the sensor over three cycles in the temperature range of 30.3 to 50 °C; **e** schematic illustration of the sensor under bending; **f** current response of the sensor over 15 bending cycles (the current change takes the absolute value); **g** current response of the sensor to the bending angle in the range of 0° to 180°(the current change takes the absolute value); **h** stability and durability of the sensor response after 1000 bending cycles°(the current change takes the absolute value).

matic of the test setup and the defined bending angle are illustrated in (Fig. 3**e**). The sensing mechanism is depended on the impedance change of the sensing layer: the bending deformation of the sensor resulted in bending and stretching of the porous CFs-MWCNT conductive sensing layer, thereby increasing the resistance. When the deformation is restored, the conductive sensing layer recovered its original state, and the resistance returned to an unbent state. Here, similar to the pressure sensitivity, we define the bending sensitivity as follows:

$$S_b = (\Delta I/I_O)/\Delta\theta \quad (3)$$

where ΔI is the corresponding current change due to bending and releasing (the current change takes the absolute value), I_O is the initial current without bending, and $\Delta\theta$ is the change of the bending angle.

The current response of the sensor under cyclic bending with a bending angle of 90 ℃ is shown in (Fig. 3**f**), demonstrating that the sensor had a stable bending response. The current response of the sensor to the bending angle (θ) in the range of 0° to 180° is presented in (Fig. 3**g**). It shows that the sensor has a good linear correlation and high sensitivity of 95.5 % rad^{-1}, corresponding to a better bending sensitivity than reported in recent work [44,45]. (Fig. 3**h**) shows the current response curve of the sensor, revealing an excellent stability and durability after 1000 bending cycles. This indicates that the flexible sensor could achieve sensitive tactile detection during curvature sensing. Importantly, the as-prepared sensor has multiple pressure/temperature/bending sensing functions to better meet actual application requirements compared to single-signal working sensors [46–49].

3.4. Detection of human motion

We attach the sensor to various active parts of the human body, including finger, wrist, elbow, knee, and heel, in order to test its effectiveness in the detection of human motion, as shown in (Fig. 4**a**). The sensors are fixed on the wrist with tape, and the wrist was cyclically bent at a certain angle to monitor the bending of the wrist in real time. The current response is shown in (Fig. 4**b**). During repeated bending and releasing of the wrist, the corresponding current is stable. The bending of the wrist deformed the sensor, and the current is increased correspondingly. Subsequently, a similar test is performed by mounting the sensor on elbow and knee joint. A unique and reproducible current signal is recorded during bending and releasing (Fig. 4**c, d**). The ability of the sensor for detecting heel pressure is depicted in (Fig. 4**e**). When the heel periodically applied pressure to the sensor, the conductive network deformed, resulting in the measured electrical signal response. (Fig. 4**f**) shows a set of gestures forming the letters “L”, “O”, “V”, and “E”. These letters are converted into current signals on different fingers by configuring the hand into the corresponding gestures. The sensors are installed on the five fingertips of a rubber glove to monitor the touch sensing of objects and enable its potential application in human robots (Fig. 4**g**). The as-prepared sensor detects the tactile stimulus of each finger, and we measure the different current signals of each gesture (e.g., five fingers touching each other). These results demonstrate the

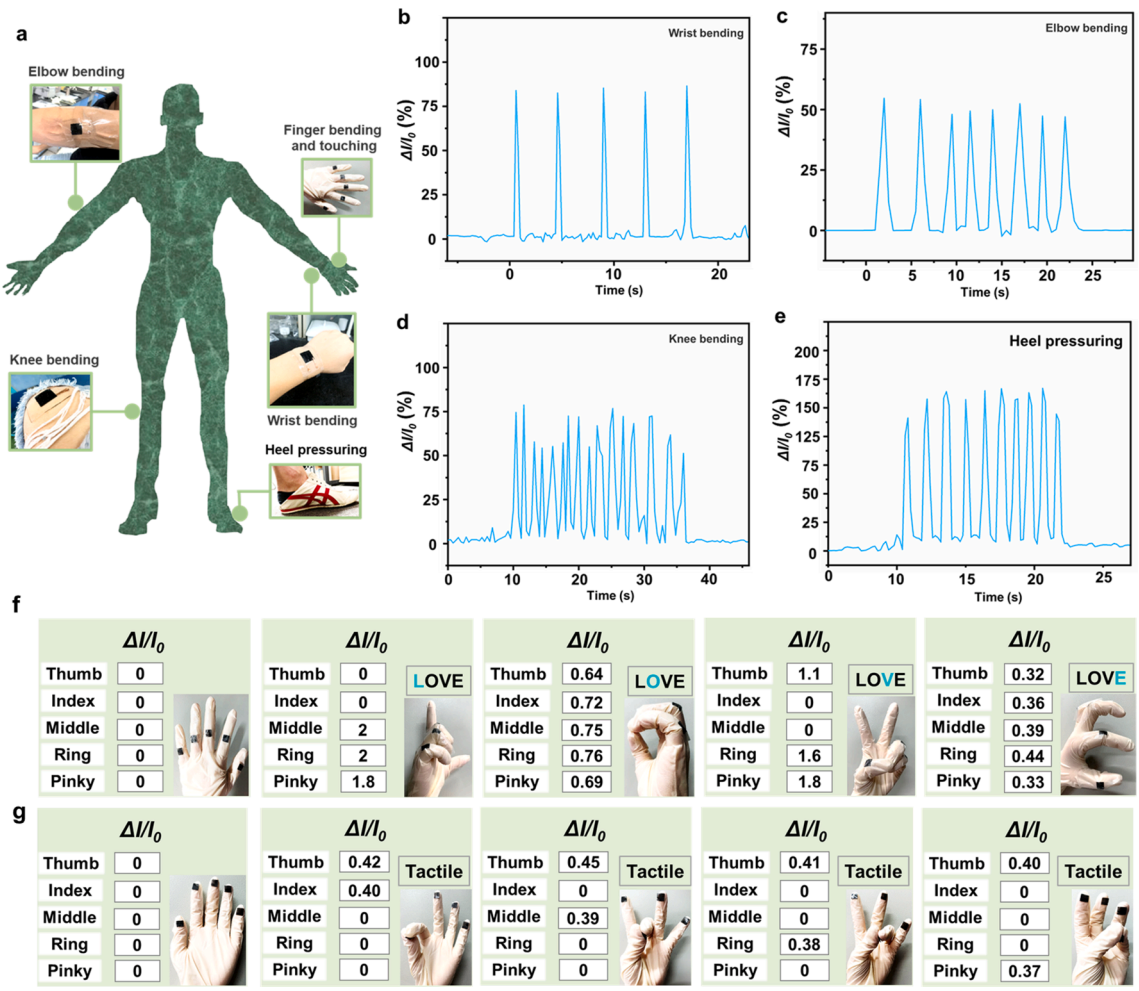

Fig. 4. Application of the sensor in the detection of human motion. **a** Overview of the sensor locations; **b–e** relative change in the current response of the sensor at different bend–release wrist motions (**b**), elbow bending (**c**), knee bending (**d**), and heel pressuring (**e**). Wearable devices for sensing and distinguishing stimuli: **f** a series of sensors were placed on the fingers to translate "LOVE" gestures, **g** a series of sensors were placed on the fingers to translate the tactile behavior between different hands.

sensitive interaction of the sensor with human activities. In short, this technology is of great significance for future wearable electronic devices, soft robots, and electronic skins.

A flexible 4 × 5 CFs-MWCNT composite sensor array has been prepared to explore potential applications in multifunctional wearable electronic products. First, copper circuits are electroplated and etched onto a transparent and flexible polyethylene terephthalate (PET) substrate (Fig. 5**a**). Then, 20 rectangular parallelepiped samples of the same size are connected to the copper circuits with conductive tape to form a flexible 4 × 5 sensing array (Fig. 5**b, c**). A mobile phone is supported by a bottle cap and then placed on a horizontally placed sensor array to detect its current distribution (Fig. 5**d**). (Fig. 5**d**) shows that the distribution of the two-dimensional normalized current response is consistent with the shape and position of the bottle cap carrying the mobile phone. Furthermore, the sensor array is fixed on the outer surface of the handhold transparent plastic tube, and the current response distribution is detected (Fig. 5**e**). (Fig. 5**e**) shows that the two-dimensional normalized current response distribution fitted well with the position of the hand that held the transparent plastic tube. In addition, hot water is introduced into the plastic water tube containing the sensor array on the surface, as shown in (Fig. 5**f**). This demonstrated that the voltage distribution reflected the presence or absence of hot water and thus the hot water level in the tube. These results prove that the as-prepared sensor could be used as a pressure/tactile/temperature multifunctional sensor for human–computer interaction and flexible wearable devices.

4. Conclusions

We have proposed a simple, low-cost method to fabricate a composite sensor of hierarchical porous carbon fibres (CFs) and multiwalled carbon nanotubes (MWCNTs), showing excellent pressure/temperature/bending multifunctional properties and outstanding mechanical properties. The sensor's hierarchical porous structure CFs–MWCNT conductive skeleton is prepared by an ice template method and acts as the sensing layer, while the elastic resin polydimethylsiloxane (PDMS) serves as the flexible substrate. The sensor exhibits a high-pressure sensitivity of 42.5 kPa (0–10 kPa) and a fast response (<100 ms) combined with a high temperature sensitivity of 2.46% $°C^{-1}$ between 30 and 40 °C and a bending sensitivity of 95.5 % rad^{-1}. It also has a good current response in the detection of the movement of human joints, indicating that it could be applied in flexible wearable devices. In addition, we demonstrate the versatility of the flexible sensor array, as it combines pressure, deformation, and temperature sensing functions and provides a high sensitivity and high durability against compression, bending, and corrosion. We believe that the hierarchical porous structure CFs-MWCNT composite sensor has great application potential in future low-cost, green, and flexible electronic devices.

CRediT authorship contribution statement

Hao Wang: Conceptualization, Data curation, Formal analysis,

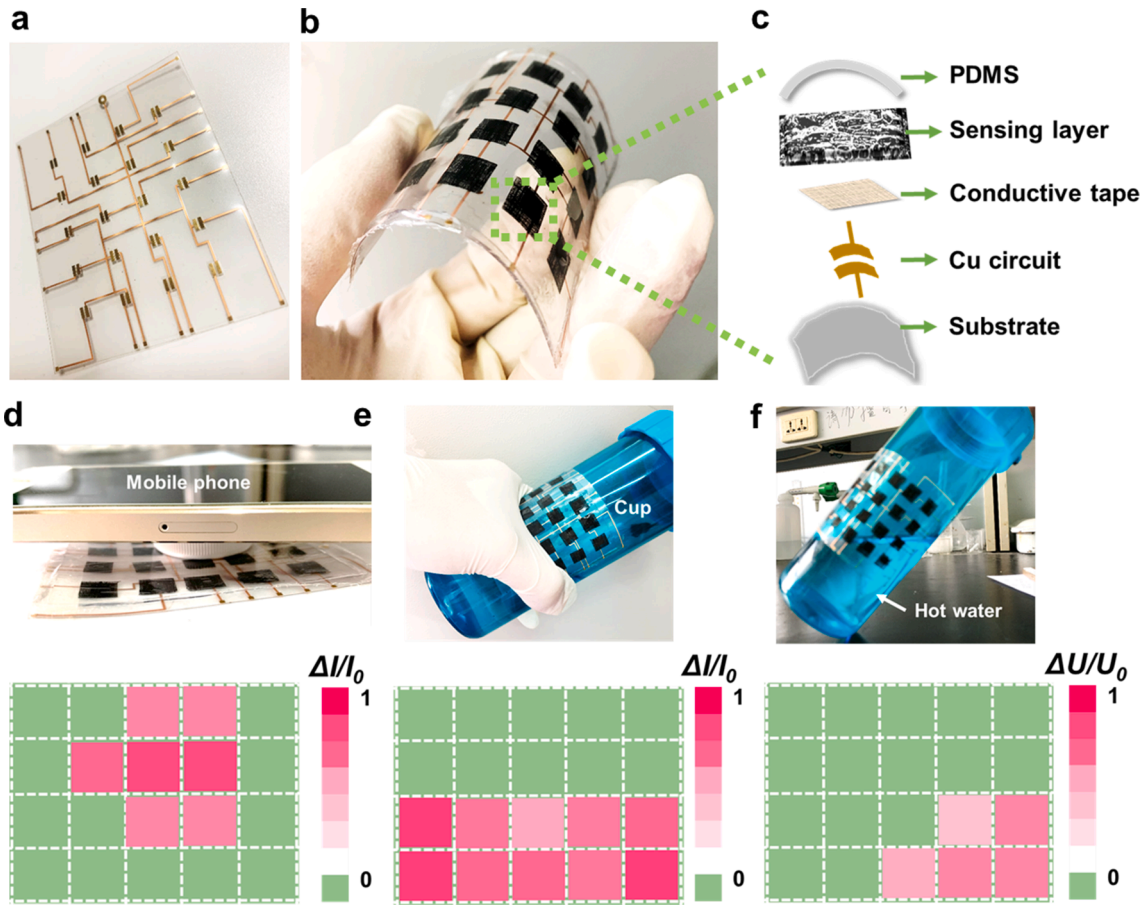

Fig. 5. Applications of the multifunctional sensing array. **a** Sensor pixel array (4 × 5) on a flexible and transparent substrate. **b** Flexible sensor array (4 × 5) based on a porous CFs-MWCNT composite material; **c** Schematic illustration of the sensing array components; **d** Mobile phone on the flat sensing array and the corresponding output current signal response; **e** Tube containing the sensor array on the surface and the corresponding output current signal response; **f** Sensor array attached to the outer surface of the transparent water tube containing hot water and the corresponding output current signal response.

Investigation, Methodology, Validation, Visualization, Writing – original draft, Writing – review & editing. **Jie Tao:** Conceptualization, Writing – review & editing, Supervision. **Kai Jin:** Investigation, Methodology, Writing – review & editing. **Xiaoyue Wang:** Data curation, Formal analysis. **Ying Dong:** Data curation, Formal analysis.

Declaration of Competing Interest

The authors declare that they have no known competing financial interests or personal relationships that could have appeared to influence the work reported in this paper.

Acknowledgements

The National Key Research and Development Program of China (No. 2017YFB0703301), the Foundation of China Scholarship Council (No. 202006830082), and the Interdisciplinary Innovation Fundation for Graduates in NUAA (No. KXKCXJJ202005).

Appendix A. Supplementary material

Supplementary data to this article can be found online at https://doi.org/10.1016/j.compositesa.2021.106796.

References

[1] Rogers JA, Someya T, Huang Y. Materials and mechanics for stretchable electronics. Science 2010;327:1603–11067.
[2] Wang C, Wang C, Huang Z, Xu S. Materials and structures toward soft electronics. Adv. Mater. 2018;30:1801368.
[3] Guo JJ, Zhou BQ, Yang CX, Dai QH, Kong LJ. Stretchable and temperature-sensitive polymer optical fibers for wearable health monitoring. Adv. Funct. Mater. 2019;29:1902898.
[4] Boutry CM, et al. A hierarchically patterned, bioinspired e-skin able to detect the direction of applied pressure for robotics. Sci. Robot. 2018;3:eaau6914.
[5] Trung TQ, Ramasundaram S, Hwang BU, Lee NE. An all-elastomeric transparent and stretchable temperature sensor for body-attachable wearable electronics. Adv. Mater. 2016;28:502–9.
[6] Shi L, et al. Highly stretchable and transparent ionic conducting elastomers. Nat. Commun. 2018;9:2630.
[7] Ge J, et al. A bimodal soft electronic skin for tactile and touchless interaction in real time. Nat. Commun. 2019;10:4405.
[8] Sun QJ, et al. Fingertip-skin-inspired highly sensitive and multifunctional sensor with hierarchically structured conductive graphite/polydimethylsiloxane foams. Adv. Funct. Mater. 2019;29:1808829.
[9] Zhou LY, Fu JZ, Gao Q, Zhao P, He Y. All-printed flexible and stretchable electronics with pressing or freezing activatable liquid-metal-silicone inks. Adv. Funct. Mater. 2020;30:1906683.
[10] Deng CH, et al. Ultrasensitive and highly stretchable multifunctional strain sensors with timbre-recognition ability based on vertical graphene. Adv. Funct. Mater. 2019;29:1907151.
[11] Chhetry A, Sharma S, Yoon H, Ko S, Park JY. Enhanced sensitivity of capacitive pressure and strain sensor based on $CaCu_3Ti_4O_{12}$ wrapped hybrid sponge for wearable applications. Adv. Funct. Mater. 2019;30:1910020.
[12] Xin L, et al. Ultracomfortable hierarchical nanonetwork for highly sensitive pressure sensor. ACS Nano 2020;14:9605–12.
[13] Ren X, Pei Ke, Peng B, Zhang Z, Wang Z, Wang X, et al. A low-operating-power and flexible active-matrix organic-transistor temperature-sensor array. Adv. Mater. 2016;28(24):4832–8.
[14] Wang Y, et al. Ultra-sensitive graphene strain sensor for sound signal acquisition and recognition. Nano Res. 2015;8:1627–36.
[15] Tan CX, et al. A high performance wearable strain sensor with advanced thermal management for motion monitoring. Nat. Commun. 2020;11:3530.

[16] Gong S, et al. A wearable and highly sensitive pressure sensor with ultrathin gold nanowires. Nat. Commun. 2014;5:3132.
[17] Lipomi DJ, Vosgueritchian M, Tee B-K, Hellstrom SL, Lee JA, Fox CH, et al. Skin-like pressure and strain sensors based on transparent elastic films of carbon nanotubes. Nat. Nanotechnol. 2011;6(12):788–92.
[18] Wang X, Xiong Z, Liu Z, Zhang T. Exfoliation at the liquid/air interface to assemble reduced graphene oxide ultrathin films for a flexible noncontact sensing device. Adv. Mater. 2015;27(8):1370–5.
[19] Yang X, Fan S, Li Y, Guo Y, Li Y, Ruan K, et al. Synchronously improved electromagnetic interference shielding and thermal conductivity for epoxy nanocomposites by constructing 3D copper nanowires/thermally annealed graphene aerogel framework. Compos A Appl Sci Manuf 2020;128:105670. https://doi.org/10.1016/j.compositesa:2019.105670.
[20] Liang C, Gu Z, Zhang Y, Ma Z, Qiu H, Gu J. Structural Design Strategies of Polymer Matrix Composites for Electromagnetic Interference Shielding: A Review. Nano-Micro Lett. 2021;13(1). https://doi.org/10.1007/s40820-021-00707-2.
[21] Wang L, Qiu H, Song P, Zhang Y, Lu Y, Liang C, et al. 3D Ti3C2Tx MXene/C hybrid foam/epoxy nanocomposites with superior electromagnetic interference shielding performances and robust mechanical properties. Compos. Part A: Appl. Sci. & Manuf. 2019;123:293–300.
[22] Zhang Y, Yan Yi, Qiu H, Ma Z, Ruan K, Gu J. A mini-review of MXene porous films: Preparation, mechanism and application. J. Mater. Sci. & Technol. 2022;103:42–9.
[23] Wegst UGK, Bai H, Saiz E, Tomsia AP, Ritchie RO. Bioinspired structural materials. Nat. Mater. 2015;14(1):23–36.
[24] Wu X, Han Y, Zhang X, Zhou Z, Lu C. Large-area compliant, low-cost, and versatile pressuresensing platform based on microcrack-designed carbon black@ polyurethane sponge for human–machine interfacing. Adv. Funct. Mater. 2016;26: 6246–56.
[25] Shin KY, Lee JS, Jang J. Highly sensitive, wearable and wireless pressure sensor using free-standing ZnO nanoneedle/PVDF hybrid thin film for heart rate monitoring. Nano Energy 2016;22:95–104.
[26] Zhu Z, Li R, Pan T. Imperceptible epidermal–iontronic interface for wearable sensing. Adv. Mater. 2018;30:1705122.
[27] He ZL, et al. Highly stretchable multi-walled carbon nanotube/thermoplastic polyurethane composite fibers for ultrasensitive, wearable strain sensors. Nanoscale. 2019;11:5884–90.
[28] Jian M, et al. Flexible and highly sensitive pressure sensors based on bionic hierarchical structures. Adv. Funct. Mater. 2017;27:1606066.
[29] Liu M, et al. Large-area all-textile pressure sensors for monitoring human motion and physiological signals. Adv. Mater. 2017;29:1703700.
[30] Sihn S, Kim RY, Kawabe K, Tsai SW. Experimental studies of thin–ply laminated composites. Compos. Sci. & Technol. 2007;67:996–1008.
[31] Yao HB, et al. A flexible and highly pressure-sensitive graphene-polyurethane sponge based on fractured microstructure design. Adv. Mater. 2013;25:6692–8.
[32] Si Y, Wang XQ, Yan CC, Yang L, Yu JY, Ding B. Ultralight biomass-derived carbonaceous nanofibrous aerogels with superelasticity and high pressure-sensitivity. Adv. Mater. 2016;28:9512–8.
[33] Gong S, Schwalb W, Wang Y, Chen Yi, Tang Y, Si J, et al. A wearable and highly sensitive pressure sensor with ultrathin gold nanowires. Nat. Commun. 2014;5(1). https://doi.org/10.1038/ncomms4132.
[34] Wu YZ, et al. A skin-inspired tactile sensor for smart prosthetics. Sci. Robot. 2018; 3:eaat0429.
[35] Choi J, Kwon D, Kim K, Park J, Orbe DD, Gu J, et al. Synergetic effect of porous elastomer and percolation of carbon nanotube filler toward high performance capacitive pressure sensors. ACS Appl. Mater. Interfaces. 2020;12(1):1698–706.
[36] Lou M, Abdalla I, Zhu M, Wei X, Yu J, Li Z, et al. Highly wearable, breathable, and washable sensing textile for human motion and pulse monitoring. ACS Appl. Mater. Interfaces. 2020;12(17):19965–73.
[37] Chen X, Liu Hu, Zheng Y, Zhai Y, Liu X, Liu C, et al. Highly compressible and robust polyimide/carbon nanotube composite aerogel for high-performance wearable pressure sensor. ACS Appl. Mater. Interfaces. 2019;11(45):42594–606.
[38] Wang Y, Wu HT, Xu L, Zhang HN, Yang Y, Wang ZL. Hierarchically patterned self-powered sensors for multifunctional tactile sensing. Sci. Adv. 2020;6:eabb9083.
[39] Li M, Chen J, Zhong W, Luo M, Wang W, Qing X, et al. Large-area, wearable, self-powered pressure–temperature sensor based on 3D thermoelectric spacer fabric. ACS Sens. 2020;5(8):2545–54.
[40] Honda W, Harada S, Arie T, Akita S, Takei K. Wearable, Human-Interactive, Health-Monitoring, Wireless Devices Fabricated by Macroscale Printing Techniques. Adv. Funct. Mater. 2014;24:3299–304.
[41] Koratkar N, Modi A, Lass E, Ajayan P. Temperature effects on resistance of aligned multiwalled carbon nanotube films. J. Nanosci. Nanotechnol. 2004;4(7):744–8.
[42] Oh JH, Hong SY, Park H, Jin SW, Jeong YR, Oh SY, et al. Fabrication of high-sensitivity skin-attachable temperature sensors with bioinspired microstructured adhesive. ACS Appl. Mater. Interfaces. 2018;10(8):7263–70.
[43] Harada S, Honda W, Arie T, Akita S, Takei K. Fully printed, highly sensitive multifunctional artificial electronic whisker arrays integrated with strain and temperature sensors. ACS Nano 2014;8(4):3921–7.
[44] Wei Y, Chen S, Li F, Lin Y, Zhang Y, Liu L. Highly stable and sensitive paper-based bending sensor using silver nanowires/layered double hydroxides hybrids. ACS Appl. Mater. Interfaces. 2015;7(26):14182–91.
[45] Zhao G, Zhang X, Cui X, Wang S, Liu Z, Deng L, et al. Piezoelectric polyacrylonitrile nanofiber film-based dual-function self-powered flexible sensor. ACS Appl. Mater. Interfaces. 2018;10(18):15855–63.
[46] Gao L, Zhu C, Li L, Zhang C, Liu J, Yu H-D, et al. All paper-based flexible and wearable piezoresistive pressure sensor. ACS Appl. Mater. Interfaces. 2019;11(28): 25034–42.
[47] Chen S, Song YJ, Ding DY, Ling Z, Xu F. Flexible and anisotropic strain sensor based on carbonized crepe paper with aligned cellulose fibers. Adv. Funct. Mater. 2018; 28:1802547.
[48] Chen ZP, Ren WC, Gao LB, Liu BL, Pei SF, Cheng HM. Three-dimensional flexible and conductive interconnected graphene networks grown by chemical vapour deposition. Nat. Mater. 2011;10:424–8.
[49] Ge G, et al. Stretchable, transparent, and self-patterned hydrogel-based pressure sensor for human motions detection. Adv. Funct. Mater. 2018;28:1802576.